THz generation by dual-color pulse in prealigned molecules

Jian Wu, Yuqi Tong, Min Li, Haifeng Pan, and Heping Zeng[†]

State Key Laboratory of Precision Spectroscopy, East China Normal University, Shanghai 200062, China

Abstract

We demonstrate that the THz generation in air from a dual-color pulse, composed of the fundamental and second-harmonic waves, can be coherently controlled by field-free molecular alignment. By tuning its time delay to properly match various molecular alignment revivals, the THz generation from the dual-color pulse can be promoted or decreased due to the spatial cross-(de)focusing effect and the alignment-dependent ionization probabilities of the prealigned diatomic molecules of air. For the dual-color pulse of orthogonally polarized fundamental and second-harmonic waves, the polarization of the generated THz radiation can be controlled by the field-free molecular alignment, which functions as a transient dynamic wave-plate for the dual-color pulse with different phase velocities for the orthogonally polarized field components. The plasma effect on the THz generation of the dual-color pulse is also observed, leading to additional intensity and polarization control of the THz radiation.

PACS number: 33.80.-b, 33.15.Bh, 42.65.-k, 52.38.-r

[†] Electronic address: hpzeng@phy.ecnu.edu.cn

Generation of electromagnetic radiation in the frequency region of terahertz (THz) has attracted ever-growing attention for its fundamental significance and interesting applications. THz generation through optical filamentation in gases [1-4] is especially promising to achieve strong THz radiations at remote targets without detrimental absorption attenuation by the presence of water vapor in air. It was demonstrated that the forward THz radiations could be enhanced by using two partially overlapped parallel filaments [5,6], static electric field biased intense filaments [7], or dual-color filaments in air [8-12]. A plasma current model was proposed to explain such enhancement of the THz generation. For instance, a nonlinear transient electron current could be formed in the filament driven by fundamental-wave (FW) and second-harmonic (SH) dual-color pulses, due to their coherently combined asymmetric laser fields that caused the electrons drifting away from the ions to acquire a nonzero drift velocity and thus resulted in simultaneous emission of THz radiation in the far-field. Owing to the highly nonlinear and phase-sensitive nature of the plasma-current-based processes, the polarization of the THz radiation could be controlled by changing the relative phase of the FW and SH dual-color pulses [13, 14]. For many important applications, it is highly desired that THz emission could be remotely controllable in an all-optical way.

Based on the intrinsic mechanism, the plasma-current-based THz generation and high harmonic generation (HHG) in gas-phase atoms or molecules are closely relevant as both involve semi-classical three-step processes [15]. The instantaneous laser field enforces rapid tunnel ionization by suppressing the atomic or molecular Coulomb barrier. The peeled electrons are accelerated under the influence of the driving laser field, and then recombine with the parent ions to give off the energy gained from the laser field in the form of high harmonics, or drift away from the parent ions to produce nonlinear electron current responsible for THz generation. Recent studies showed that the HHG could be controlled by manipulating the electron wave-packet dynamics with molecular alignment [16] and that tomographic

reconstruction of the highest occupied molecular orbital was accomplished by high harmonics generated from intense fs pulses focused on aligned molecules [17]. It is of fundamental interest to examine how molecular alignment affects the nonlinear electron current and whether THz generation can be controlled in the molecular alignment wakes.

In this work, we reveal some unique effects of molecular alignment on THz generation driven by dual-color filaments in air. By matching the dual-color pulses to appropriate revivals of the molecular alignment created by an advancing collinear molecular-alignment pulse (M-pulse), we experimentally demonstrate that THz radiation can be remotely controlled in an all-optical way and that the THz intensities and polarization states can be changed with the molecular alignment revivals. Different mechanisms were verified robust for the all-optical control of the THz generation. Molecular alignment was demonstrated to induce spatial cross-phase modulation (XPM) that affected the intense fs filament dynamics, where the alignment effects such as alignment-induced (de)focusing competed or cooperated with the plasma defocusing and Kerr self-focusing. Plasma density and plasma current changed with the molecular alignment due to the alignment-dependent ionization cross sections of the air molecules, while the ultrafast change of the refractive index during the molecular alignment revivals shifted the relative phase of the orthogonally polarized components of the dual-color pulses and thus induced observable changes of the combined asymmetric electric fields, resulting in an alignment-dependent polarization rotation of the generated THz. All those effects can be used to control the THz generation, which offer convenient all-optical methods to control the dual-color-driven THz generation by properly aligning the air molecules.

The experiments were performed with a Ti:sapphire amplifier at 800 nm of 1 kHz repetition rate. The 50-fs output pulse with the pulse energy of ~2.3 mJ was split into strong and weak ones with the energy ratio of 2:1. The strong FW pulse was focused by a positive lens of f=60 cm into a 200-μm-thick type-I β-BBO crystal to

produce the FW and SH dual-color pulse for THz generation in air. The FW and SH phase lag was compensated by using an x-cut 2.5-mm-thick α-BBO crystal as the birefringence plate, and their relative polarization was adjusted by using a dual-wavelength wave-plate. The weak M-pulse with a tunable time delay for air molecular alignment was focused by a positive lens of f=80 cm, which was then collinearly combined with the dual-color pulse after a thin film polarizer (TFP). The M-pulse energy was adjusted by using a half wave-plate before the TFP which only reflected the s-polarized component. The focuses of the M-pulse and dual-color pulse were adjusted to spatially overlap. At the end of the filament, a 3-mm-thick Teflon filter was used to block the laser pulses. The transmitted THz radiation was then collected and focused into a 1.5-mm-thick ZnTe crystal [(110) cut] by two gold-coated parabolic mirrors. The THz electric field was then characterized by a standard electro-optic (EO) sampling measurement with a weak FW pulse leakage after a high-reflective mirror as the probe. A wire grid THz polarizer was inserted between the parabolic mirrors to analyze the polarization of the generated THz radiation [18].

We concentrated on the FW and SH dual-color pulses of parallel and orthogonal polarizations, denoted by FW//SH and FW□SH, respectively. We firstly studied the THz generation from the dual-color pulse with parallel polarized FW and SH components (FW//SH) in pre-aligned air molecules. The FW and SH pulse energies in the dual-color pulse were measured to be 0.94 and 0.14 mJ, respectively. Figure 1(a) shows the measured THz intensity as a function of the M-pulse time delay, where the EO sampling probe pulse was fixed at the peak of the THz electric field waveform, and the transmission direction of the wire grid THz polarizer was set parallel to the dual-color pulse polarization. The negative (positive) time delay accounts for the dual-color pulse was ahead (behind) the M-pulse. Figure 1(b) shows the simulated molecular alignment [19] signal $\langle\langle\cos^2\theta_\perp\rangle\rangle$ of air, where $\theta_\perp$ is the angle between the molecular axis and the direction perpendicular to the M-pulse polarization. The molecules were firstly aligned perpendicularly to the dual-color pulse polarization, and then revived periodically with periods of 8.6 and 11.3 ps for N_2 and O_2, respectively.

Around zero time delay, the XPM between the orthogonally polarized M-pulse

and dual-color pulse induced a refractive index increase as $\delta n_{Kerr}(r)=2n_2/3I_M(r)$, where n_2 is the Kerr nonlinear coefficient of air [20, 21]. The dual-color pulse experienced an XPM-induced focusing of the spatial profile proportional to M-pulse intensity $I_M(r)$ and thus the dual-color pulse intensity increased in the interaction region. Accordingly, the THz generation was enhanced around the zero time delay.

After the zero time delay, the M-pulse induced plasma with a negative refractive index change ($\delta n_{plas}\sim-\rho/2\rho_{cr}$, where ρ is the electron density of plasma and $\rho_{cr}\sim\lambda^{-2}$ is the critical density connecting with the laser wavelength λ) introduced a cross plasma-defocusing effect, which reduced the dual-color pulse intensity and hence decreased the THz generation. The higher plasma density (by using a higher M-pulse energy) was, the more the THz intensity decreased. As the M-pulse energy was increased to 0.6 mJ, as shown in Fig. 1(a), the baseline of the THz intensity decreased due to the plasma defocusing effect induced by the M-pulse ahead the dual-color pulse.

THz generation was then modulated periodically along the periodic molecular alignment revivals [see Fig. 1(b)]. The refractive index of the pre-aligned molecules was changed by following $\delta n_{mol}(r,t)\sim2\pi\rho_0\Delta\alpha/n_0[<<\cos^2\theta_\perp(r,t)>>-1/3]$ [21], where $\Delta\alpha$, ρ_0, and n_0 denote the molecular polarizability difference, initial molecular number density, and linear refractive index of the randomly orientated molecules, respectively. As the Gaussian-shaped transverse profile of the M-pulse induced a larger molecular alignment degree at the beam center, perpendicularly aligned molecules with $<<\cos^2\theta_\perp>>-1/3<0$ caused a cross-defocusing for the dual-color pulse, resulting in a decrease of the THz generation due to decrease of the dual-color pulse intensity. Meanwhile, the ionization probability of the perpendicular aligned molecules was reduced for the lack of the double-well potential [16,22], which on the other hand reduced the plasma density as well as the plasma current, and accordingly decreased the THz generation driven by the dual-color pulse. In the contrast, parallel aligned molecules with $<<\cos^2\theta_\perp>>-1/3>0$ introduced a cross-focusing effect to the dual-color pulse for its positive refractive index change, which meanwhile increased the ionization probabilities of the diatomic molecules [16,22]. The increased field intensity of the dual-color pulse and ionization probability of the diatomic molecules led to the increase of the THz generation. Consequently, as shown in Fig. 1(a), the

THz intensity was observed to increase or decrease by closely following the periodic revivals of the parallel or perpendicular molecular alignment. By pre-aligning the air molecules with the M-pulse energy of 0.47 mJ, an enhancement of 15% of the THz intensity was observed at the parallel molecular alignment revival at delay C. Figure 1(d) shows the THz waveform at various time delays of the M-pulse as labeled in Fig. 1(a), where no noticeable changes of the THz waveform shape and peak location were observed. The transverse fluorescence emitted from the dual-color pulse induced plasma was also measured [23] by a photomultiplier tube (PMT) after a serial of filters including two broadband high reflective mirrors centered at 400 and 800 nm, two band-pass filters (transmission from 250 to 380 nm), and an UG11 color-glass filter (transmission from 200 to 400 nm). As expected, the fluorescence intensity periodically modulated [20] as shown in Fig. 1(c), by following the revivals of the molecular alignment when the time delay between the M-pulse and dual-color pulse was tuned.

There was a cooperation or competition between the molecular alignment, plasma, and Kerr effects on the THz generation. As shown in Fig. 1(a), the molecular alignment induced modulation of the THz intensity became more observable as the M-pulse energy was increased to enhance the molecular alignment degree. Meanwhile, the overall THz intensity was somehow decreased due to the plasma defocusing effect when the M-pulse energy increased. This became much more observable for the perpendicular molecular alignment revivals, where the plasma effect and the molecular alignment cooperated to defocus the dual-color pulse for the THz generation. Figure 1(e) shows the measured THz intensity as a function of the M-pulse energy for two selected time delays C and D (1/2 revival of N_2) as labeled in Fig. 1(a). Taking the parallel molecular alignment revival at delay C as an example, for a low M-pulse intensity of $I_M \sim 1.5\times10^{13}$ W/cm^3, the refractive index changes by the molecular alignment and plasma were estimated to be $\delta n_{mol} \sim 0.35\times10^{-5}$ and $\delta n_{plas\_FW} \sim -3.08\times10^{-9}$ and $\delta n_{plas\_SH} \sim -7.69\times10^{-10}$ for a polarizability difference of $\Delta\alpha \sim 1.0$ Å^3 (electrostatic units) and plasma density of $\rho \sim 1.08\times10^{13}$ cm^{-3}, respectively. The plasma effect was negligibly small and the THz generation was actually dominated by the molecular alignment effect. However, the plasma effect became noticeable for the M-pulse intensity of $I_M \sim 5.0\times10^{13}$ W/cm^3, where the refractive index changes by the molecular alignment and plasma were estimated to be $\delta n_{mol} \sim 1.21\times10^{-5}$ and

$\delta n_{plas\_FW} \sim -1.11\times10^{-5}$ and $\delta n_{plas\_SH} \sim -0.28\times10^{-5}$ for a plasma density of $\rho=3.89\times10^{16}$ cm^{-3}, respectively. As shown in Fig. 1(e) at delay C, an optimal THz enhancement was observed around the M-pulse energy of ~0.4 mJ and could be attributed to the competition between the parallel molecular alignment revival (cross-focusing) and plasma effect (cross-defocusing). The THz intensity decreased gradually as the increase of the M-pulse energy for the perpendicular molecular alignment revival at delay D, where the plasma effect cooperated with the molecular alignment to decrease the THz generation.

The THz generation in the pre-aligned air molecules was more interesting when the FW and SH components of the dual-color pulse were orthogonally polarized (FW ⊥SH). The FW and SH components of 1.0 and 0.11 mJ in the dual-color pulse were set to be perpendicular and parallel to the M-pulse polarization, respectively. For this orthogonal polarization case, we defined the parallel (perpendicular) molecular alignment as the molecule axis was parallel (perpendicular) to the polarization of the FW components. Figure 2(a) shows the measured THz intensity from the dual-color pulse (FW⊥SH) as a function of the M-pulse time delay. The transmission direction of the wire grid THz polarizer was parallel to the polarization of the SH component of the dual-color pulse. The time delay between the probe and THz pulses was fixed at peak P as labeled in Fig. 2(b). The THz generation exhibited a periodic intensity modulation similar to the molecular alignment revivals. As the FW component was more intense than the SH component, the THz intensity modulation followed the alignment-induced cross-(de)focusing effect of the FW pulse.

Interestingly, as shown in Fig. 2(a), the THz amplitude became negative for the perpendicular molecular alignment revivals, such as those at delays B, D, and F. It was due to the time shift of the THz waveform as shown in Fig. 2(b) (for the case at delay B). This kind of waveform change caused the polarization rotation of the THz radiation as shown in Fig. 3(a). It has been recently demonstrated [13,14] that the THz polarization from a dual-color pulse of differently polarized FW and SH components could be controlled by changing the relative phase between the FW and SH components. Here, as shown in Fig. 3(a), the observed THz polarization rotation could be understood in a similar way. For the perpendicular molecular alignment revivals with molecular axis perpendicular to the FW polarization but parallel to the

SH polarization, the refractive index was decreased and increased for the FW and SH components, which increased and decreased the propagation velocities of the FW and SH components, respectively. Meanwhile, the refractive index decrease induced by the plasma was four times larger for the FW pulse than that for the SH one, which made the FW component to propagate faster than the SH one. As shown in Fig. 3(a) at delay D, this cooperation between the perpendicular molecular alignment revival and plasma effect significantly rotated the THz polarization as compared to the case at the time delay H ahead the M-pulse [see Fig. 3(a)]. However, for the parallel molecular alignment revival, the refractive index was increased and decreased for the FW and SH components, respectively, which decreased and increased the propagation velocities of the FW and SH components and might counterbalance the propagation velocity difference introduced by the plasma effect. As a result, as shown in Fig. 3(a) for the parallel molecular alignment revivals at delay C, the polarization rotation was small in comparison with the case at delay D. The plasma effect on the THz polarization rotation was also observed as shown in Fig. 3(a) at delay E for a relatively high M-pulse energy with a noticeable plasma density.

The competition and cooperation between the molecular alignment and plasma effects could be further identified by changing the M-pulse energy. As shown in Fig. 3(a) at delay C, the polarization changes were small as the increase of the M-pulse energy due to the competition between the parallel molecular alignment revivals and plasma effect. However, as shown in Fig. 3(a) at delay D, the THz polarization was rotated significantly as the M-pulse energy was increased due to the cooperation between the perpendicular molecular alignment revivals and plasma effect. As shown in Fig. 3(a) at delay H, almost no changes of the THz polarization were observed as the M-pulse energy varied, since this time delay was set before the coming of the M-pulse. Figure 2(c) shows the dependence of the THz intensity (along the SH polarization) on the M-pulse energy. For the parallel molecular alignment revival at delay C, the molecular alignment effect made the THz intensity increase with the M-pulse energy in the low M-pulse energy range where the plasma effect was negligibly small. Nevertheless, in the high M-pulse energy range where the plasma effect played a significant role, the THz intensity decreased with the increase of the M-pulse energy. An optimal THz enhancement was observed for M-pulse energy of ~0.4 mJ and could be attributed to the competition between the parallel molecular

alignment and plasma effects. As shown in Fig. 2(c), a similar evolution trend of the THz field amplitude was observed for the perpendicular alignment revival at delay D, where the negative value of the THz field amplitude was due to the time shift of the THz waveform related to the THz polarization rotation as shown in Fig. 3(a) at delay D. For the case of parallel polarized FW and SH components that experienced the same molecular alignment direction, as shown in Fig. 3(b), the THz radiation was almost linearly polarized, and no noticeable rotation of the THz polarization was observed either the relative time delay or the pulse energy of the M-pulse was changed.

In summary, we experimentally demonstrated that THz radiation generated by dual-color pulse in air could be coherently controlled by field-free molecular alignment. By tuning the time delay of the dual-color pulse to properly match the molecular revival or varying the M-pulse energy, the THz generation could be promoted or decreased. For the dual-color pulse of orthogonally polarized FW and SH components, the THz polarization could be rotated by the field-free molecular alignment and ionization-induced plasma effect, which functioned as a transient wave-plate in the THz frequency range. This field-free control of THz radiation might find promising applications in THz-based remote sensing in air.

This work was partly funded by National Natural Science Fund (10525416 and 10804032), National Key Project for Basic Research (2006CB806005), and Projects from Shanghai Science and Technology Commission (08ZR1407100 and 09QA1402000).

References:

[1] H. Hamster, A. Sullivan, S. Gordon, W. White, and R.W. Falcone, Phys. Rev. Lett. **71**, 2725 (1993).

[2] C. Cheng, E M. Wright, and J.V. Moloney, Phys. Rev. Lett. **87**, 213001 (2001).

[3] P. Sprangle, J. R. Peñano, B. Hafizi, and C. A. Kapetanakos, Phys. Rev. E **69**, 066415 (2004).

[4] W. Hoyer, A. Knorr, J. V. Moloney, E. M. Wright, M. Kira, and S. W. Koch, Phys. Rev. Lett. **94**, 115004 (2005).

[5] Y. Liu, A. Houard, B. Prade, S. Akturk, A. Mysyrowicz, and V. T. Tikhonchuk, Phys. Rev. Lett. **99**, 135002 (2007).

[6] M. Durand, Y. Liu, A. Houard, and A. Mysyrowicz, Opt. Lett. **35**, 1710 (2010).

[7] A. Houard, Y. Liu, B. Prade, V. T. Tikhonchuk, and A. Mysyrowicz, Phys. Rev. Lett. **100**, 255006 (2008).

[8] D. J. Cook and R. M. Hochstrasser, Opt. Lett. **25**, 1210 (2000).

[9] M. Kress, T. Löffler, S. Eden, M. Thomson, and H. G. Roskos, Opt. Lett. **29**, 1120 (2004).

[10] T. Bartel, P. Gaal, K. Reimann, M. Woerner, and T. Elsaesser, Opt. Lett. **30**, 2805 (2005).

[11] X. Xie, J. Dai, and X. C. Zhang, Phys. Rev. Lett. **96**, 075005 (2006).

[12] Y. Chen, M. Yamaguchi, M. Wang, and X. C. Zhang, Appl. Phys. Lett. **91**, 251116 (2007).

[13] H. Wen and A. M. Lindenberg, Phys. Rev. Lett. **103**, 023902 (2009).

[14] J. Dai, N. Karpowicz, and X. C. Zhang, Phys. Rev. Lett. **103**, 023001 (2009).

[15] P. B. Corkum, Phys. Rev. Lett. **71**, 1994 (1993).

[16] T. Kanai, S. Minemoto, and H. Sakai, Nature **435**, 470 (2005).

[17] J. Itatani, J. Levesque, D. Zeidler, H. Niikura, H. Pépin, J. Kieffer, P. Corkum, and D. Villeneuve, Nature **432**, 867 (2004).

[18] P. C. M. Planken, H. K. Nienhuys, H. J. Bakker, and T. Wenckebach, J. Opt. Soc. Am. B **18**, 313 (2001).

[19] H. Stapelfeldt and T. Seideman, Rev. Mod. Phys. **75**, 543 (2003).

[20] J. Wu, H. Cai, P. Lu, X. Bai, L. Ding, and H. Zeng, Appl. Phys. Lett. **95**, 221502 (2009).

[21] J. Wu, Y. Tong, X. Yang, H. Cai, P. Lu, H. Pan, and H. Zeng, Opt. Lett. **34**, 3211

(2009).

[22] J. Wu, H. Zeng, and C. Guo, Phys. Rev. A **74**, 065403 (2006); **75**, 043402 (2007).

[23] H. Cai, J. Wu, H. Li, X. Bai, and H. Zeng, Opt. Express **17**, 21060 (2009).

Figure captions

Figure 1 (color online) (a) The measured THz intensity from the parallel polarized dual-color pulse as a function of the M-pulse time delay for various M-pulse energies. (b) The simulated impulsive molecular alignment signal of N_2 and O_2 in air observed along the direction perpendicular to the M-pulse polarization. (c) The measured fluorescence intensity emitted from the dual-color filament as a function of the M-pulse time delay. (d) The measured THz waveforms when the dual-color pulse was tuned to match different time delays for M-pulse energy of ~0.47 mJ. (e) The measured THz intensity from the dual-color pulse as a function of the M-pulse energy for different molecular alignment revivals.

Figure 2 (color online) (a) The measured THz intensity from the orthogonally polarized dual-color pulse as a function of the M-pulse time delay for various M-pulse energies. (b) The measured THz waveforms when the dual-color pulse was tuned to match different time delays for M-pulse energy of ~0.3 mJ. (c) The measured THz intensity from the dual-color pulse as a function of the M-pulse energy for different molecular alignment revivals.

Figure 3 (color online) The measured polarizations of the THz driven by (a) FW□SH, and (b) FW//SH dual-color pulse at various M-pulse delays and energies. The M-pulse energies in (a) were ~0.2 mJ (black-squares), ~0.4 mJ (red-circles), and ~0.6 mJ (blue-triangles), and in (b) were ~0.27 mJ (black-squares), ~0.47 mJ (red-circles), and ~0.6 mJ (blue-triangles), respectively.

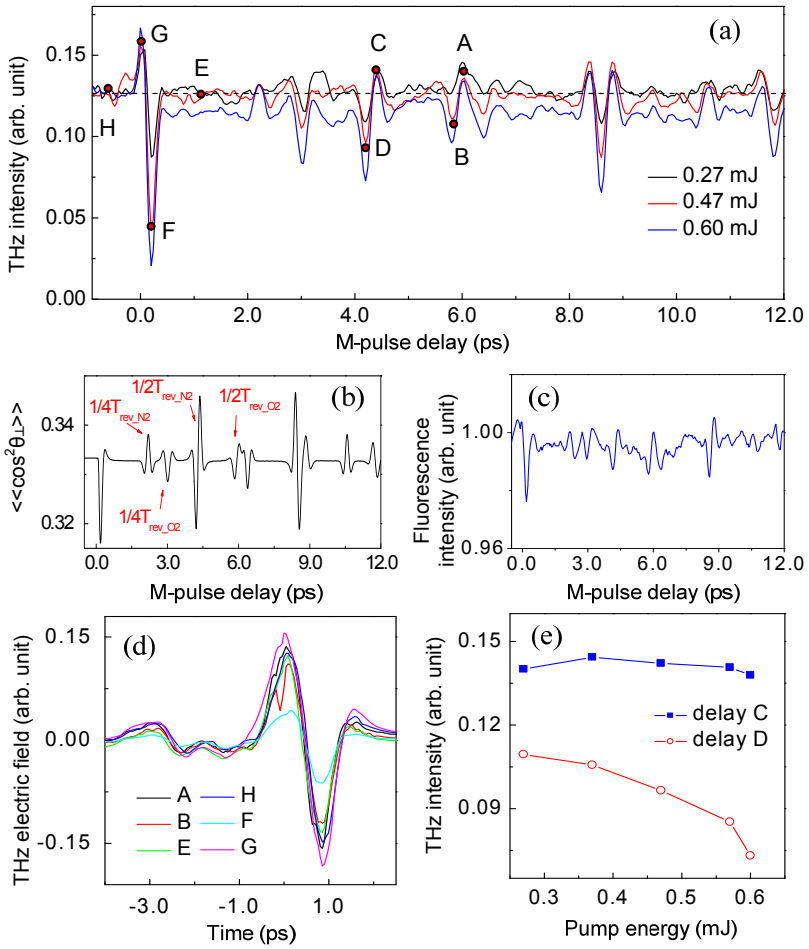

Figure 1 (color online) (a) The measured THz intensity from the parallel polarized dual-color pulse as a function of the M-pulse time delay for various M-pulse energies. (b) The simulated impulsive molecular alignment signal of N_2 and O_2 in air observed along the direction perpendicular to the M-pulse polarization. (c) The measured fluorescence intensity emitted from the dual-color filament as a function of the M-pulse time delay. (d) The measured THz waveforms when the dual-color pulse was tuned to match different time delays for M-pulse energy of ~0.47 mJ. (e) The measured THz intensity from the dual-color pulse as a function of the M-pulse energy for different molecular alignment revivals.

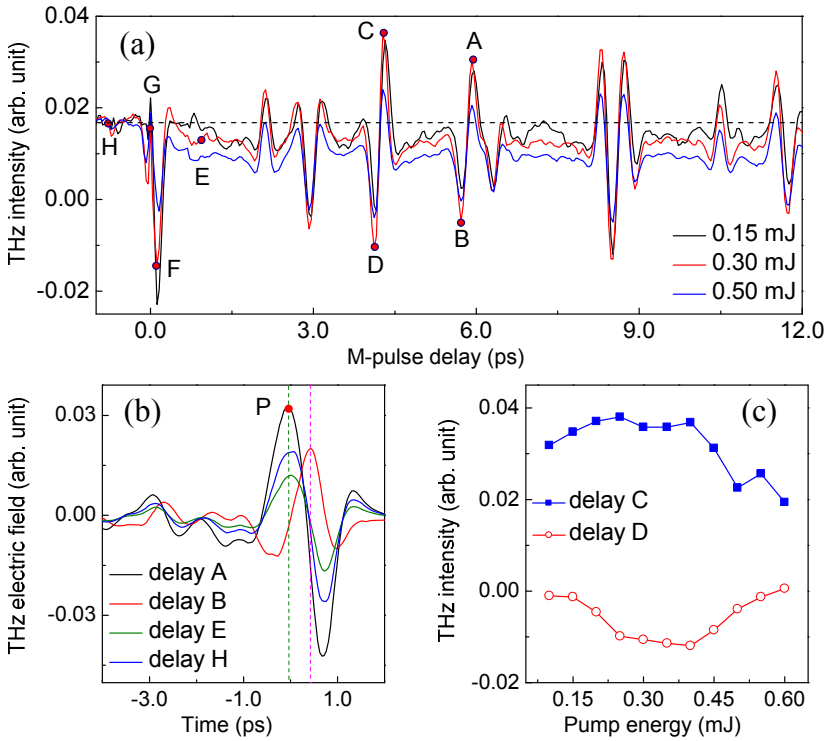

Figure 2 (color online) (a) The measured THz intensity from the orthogonally polarized dual-color pulse as a function of the M-pulse time delay for various M-pulse energies. (b) The measured THz waveforms when the dual-color pulse was tuned to match different time delays for M-pulse energy of ~0.3 mJ. (c) The measured THz intensity from the dual-color pulse as a function of the M-pulse energy for different molecular alignment revivals.

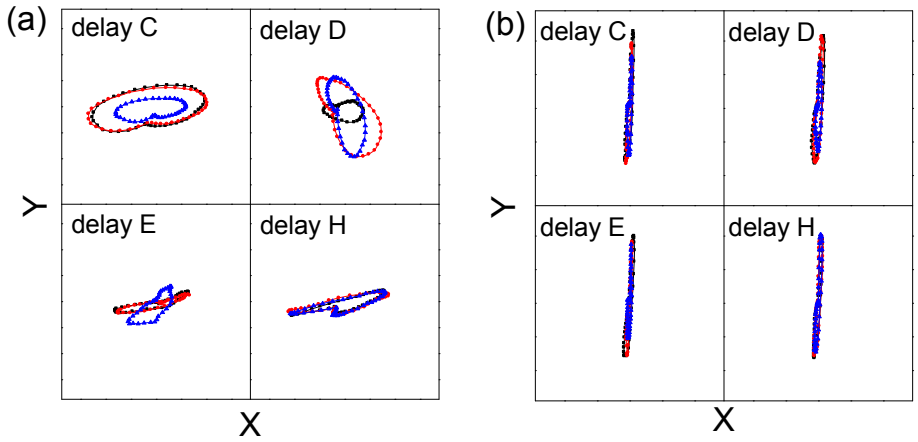

Figure 3 (color online) The measured polarizations of the THz driven by (a) FW□SH, and (b) FW//SH dual-color pulse at various M-pulse delays and energies. The M-pulse energies in (a) were ~0.2 mJ (black-squares), ~0.4 mJ (red-circles), and ~0.6 mJ (blue-triangles), and in (b) were ~0.27 mJ (black-squares), ~0.47 mJ (red-circles), and ~0.6 mJ (blue-triangles), respectively.